3D Mathematical modeling of glioblastoma suggests that transdifferentiated vascular endothelial cells promote resistance to current standard-of-care therapy

Supplemental Materials

Sec. S1. Colored figures in the Main Text.

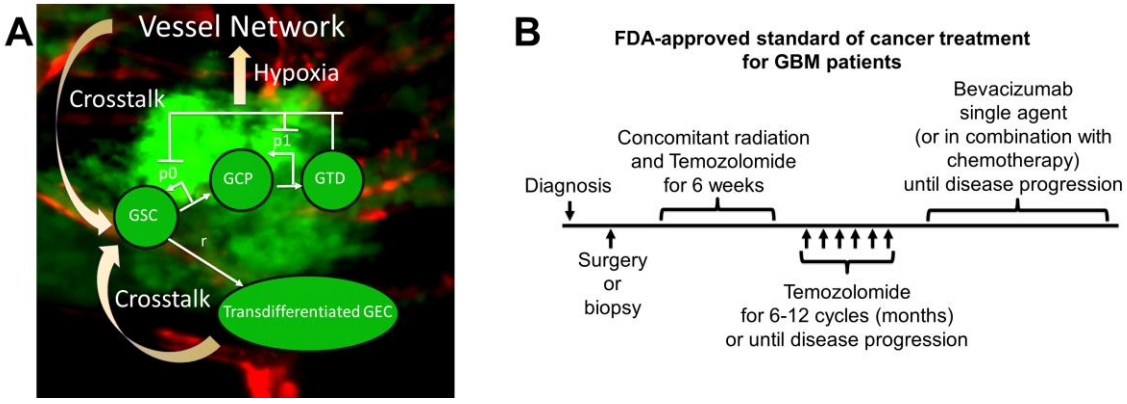

Fig. S1. Schematic of the cancer model and the standard-of-care treatment regimen for GBM patients. **(A)** Image of vascularized GBM and model schematic. GBM cells (U-87, GFP-transduced (green)), along with endothelial cells (EC, m-Cherry transduced (red)) and fibroblasts were grown in a microfluidic device. After 4 to 6 days, the endothelial cells develop a fully formed vascular network, which is perfused by cell media. **(B)** FDA-approved standard of cancer treatment for GBM patients. After surgery or biopsy is performed following diagnosis, six weeks of concomitant radiation and temozolomide are applied. Then, temozolomide is applied for 6-12 cycles (months) or until disease progression (McDonald criteria, i.e. tumor grows more than 25% of surface area). Afterwards, bevacizumab is applied as single agent or in combination with chemotherapy until disease progression.

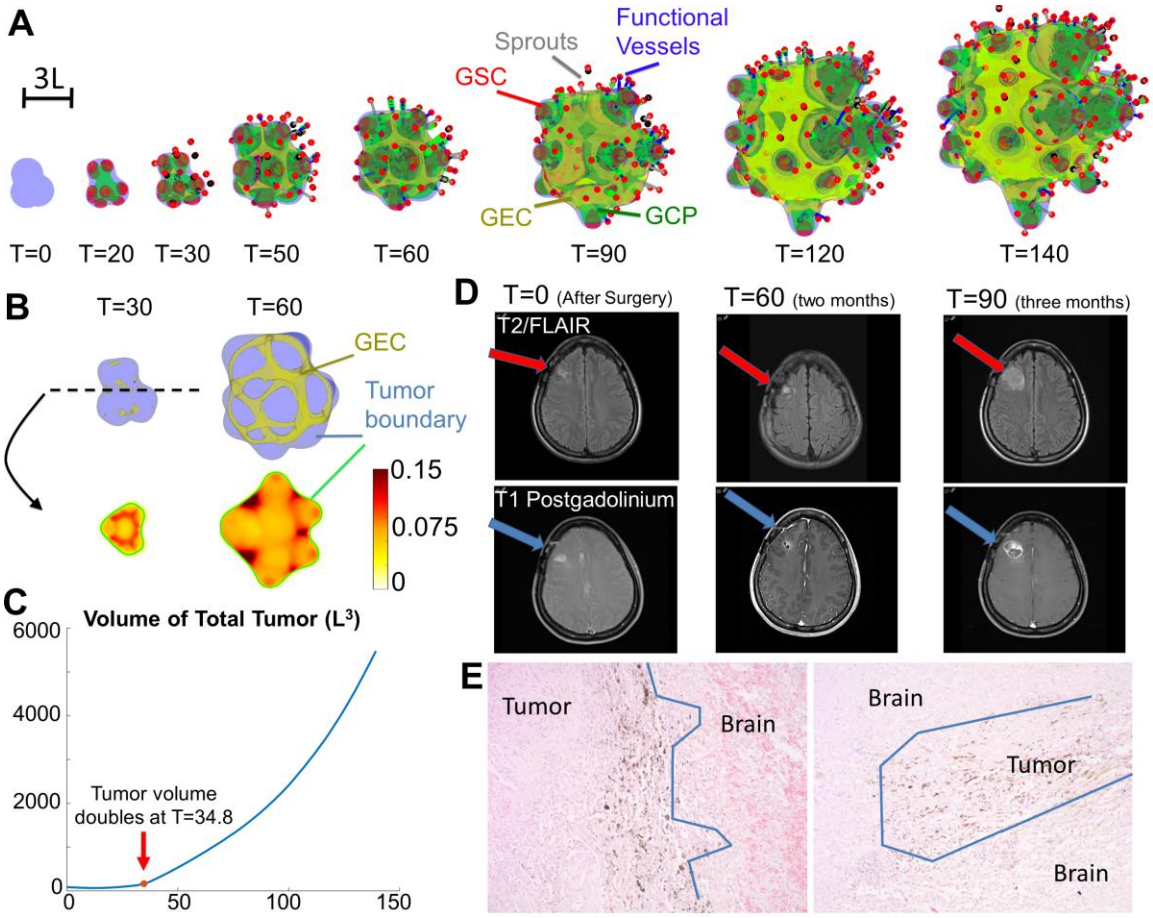

Fig. S2. Evolution of untreated vascular tumor. **(A)** Spatial distribution of tumor cells (blue: tumor boundary; red: φ_{GSC}=0.3; green: φ_{GCP}=0.25; yellow: φ_{GEC}=0.1) and vasculature (red dots: vessel initiation points; grey: vessel sprouts; blue: functional vessels; green dots: anastomosis points). **(B)** Transdifferentiated GEC spontaneously form a network structure. Top: 3D isosurfaces of tumor boundary (blue) and φ_{GEC}=0.1 (yellow) at T=30 and T=60. Bottom: 2D slices of φ_{GEC} at the center of computational domain. **(C)** Time evolution of total tumor volume. L is the diffusional length scale ($\approx 250\mu m$). At T=34.8, tumor volume doubles from T=0 (after surgery). **(D)** Exponential growth and central cavitation in a patient that declined treatment. Without treatment, tumor volume can double in 2-4 weeks. Two months after surgery, residual enhancement is gradually enlarging and more than doubled in size three months after

surgery. **(E)** GBM infiltrates the normal brain. GSCs are positioned at the edge of the invading zone. Patient tumors, IHC staining with GSC marker, TRIM 11 (1).

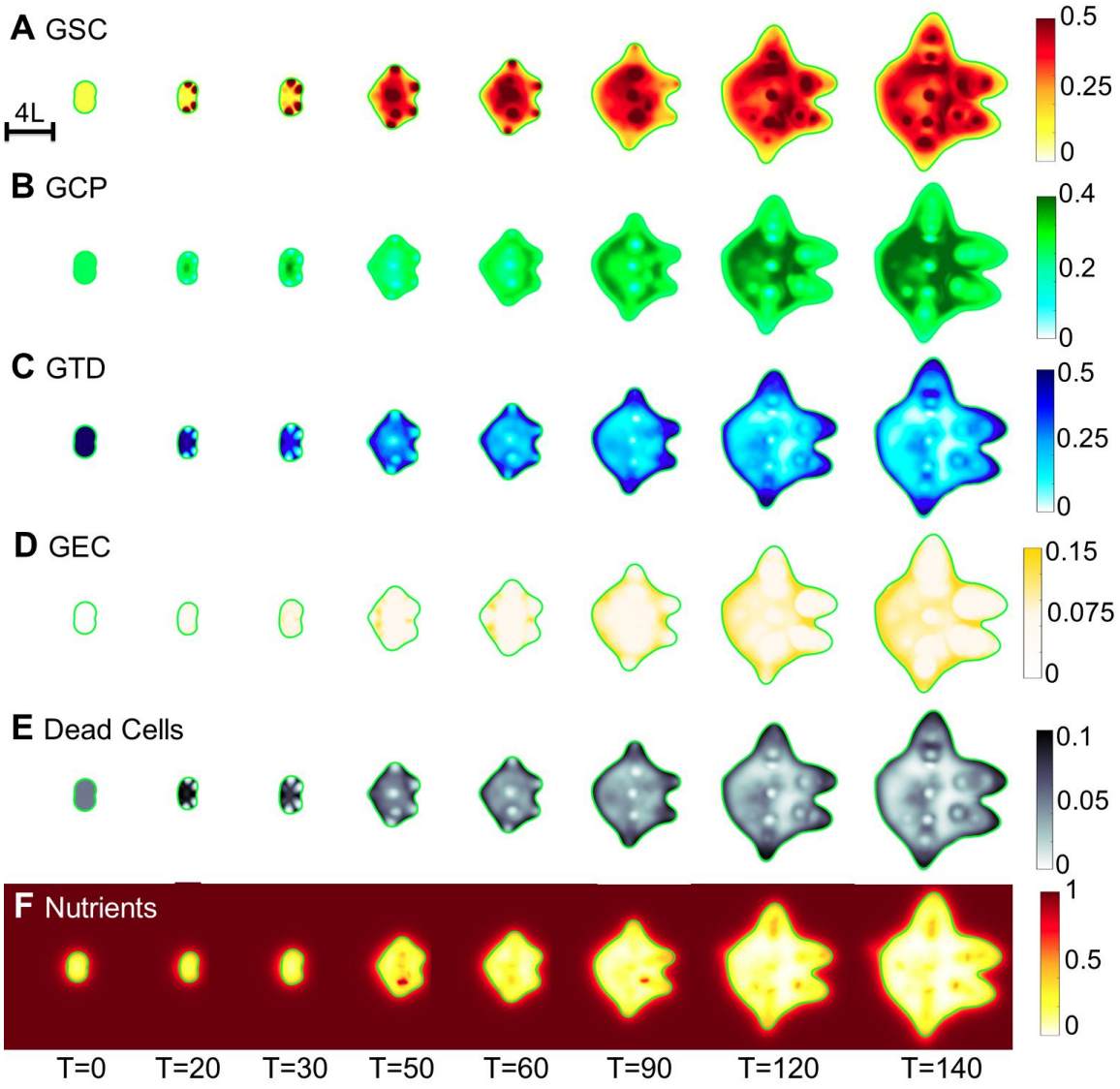

Fig. S3. Detailed analysis of the untreated vascular tumor in Fig. S2A. **(A-E)** Volume fraction of GSC, GCP, GTD, GDCs and GEC. Insets show the corresponding cell type. **(F)** Most transdifferentiated GEC locate within the hypoxic core (nutrient level less than half of that in background vasculature).

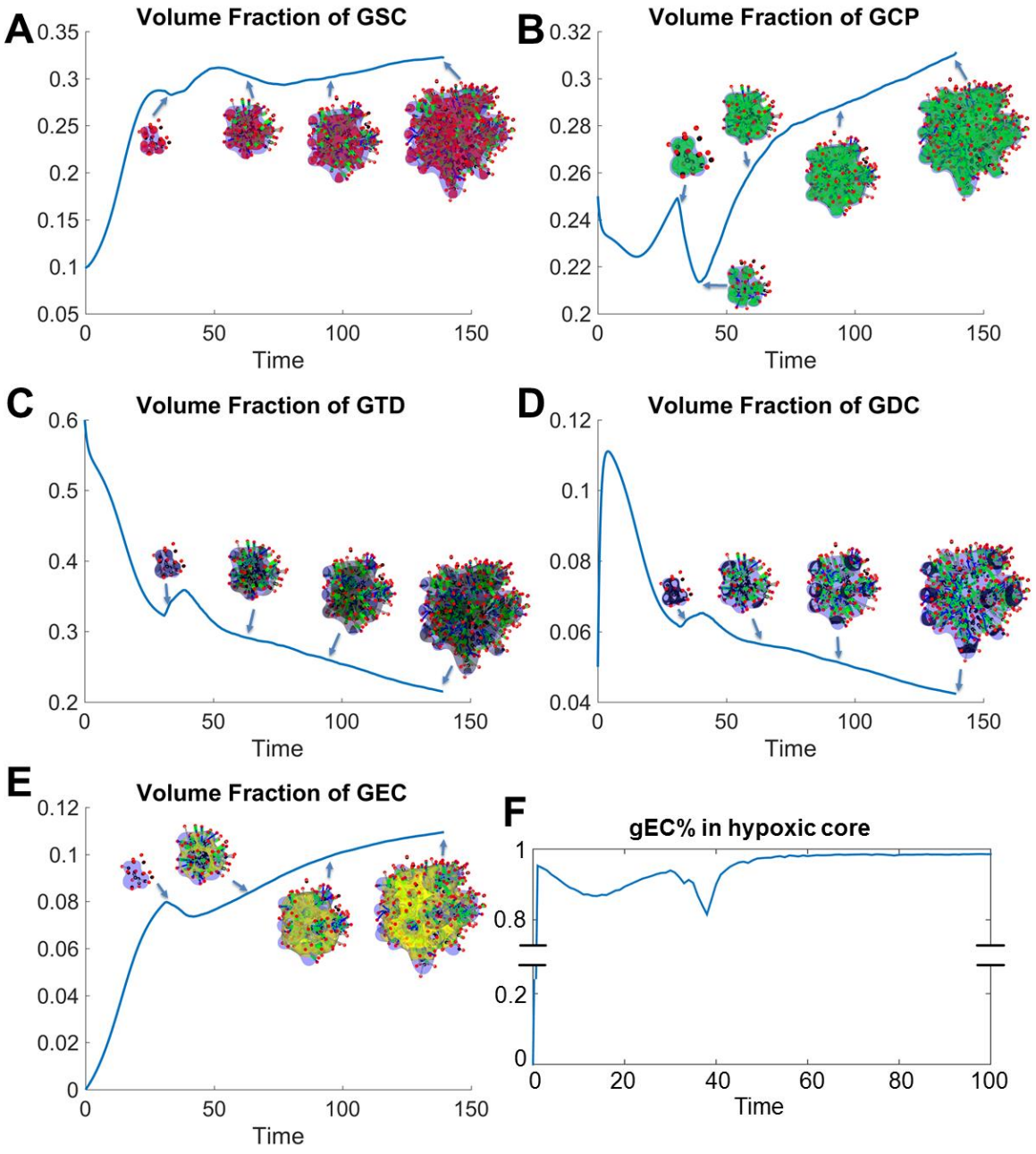

Fig. S4. 2D slices of the untreated vascular tumor in Fig. S2A. **(A-H)** Distributions of GSCs, GCPs, GTDs, GECs, dead cells, nutrients, vascular-produced GSC promoter (C_F) and vessel density at the center of the tumor. After the vasculature forms, functional vessels release nutrients in the tumor, and several new GSC clusters emerge at the tumor interior. In (D), GEC spontaneously form a network structure in the tumor, as seen in Fig. S2B.

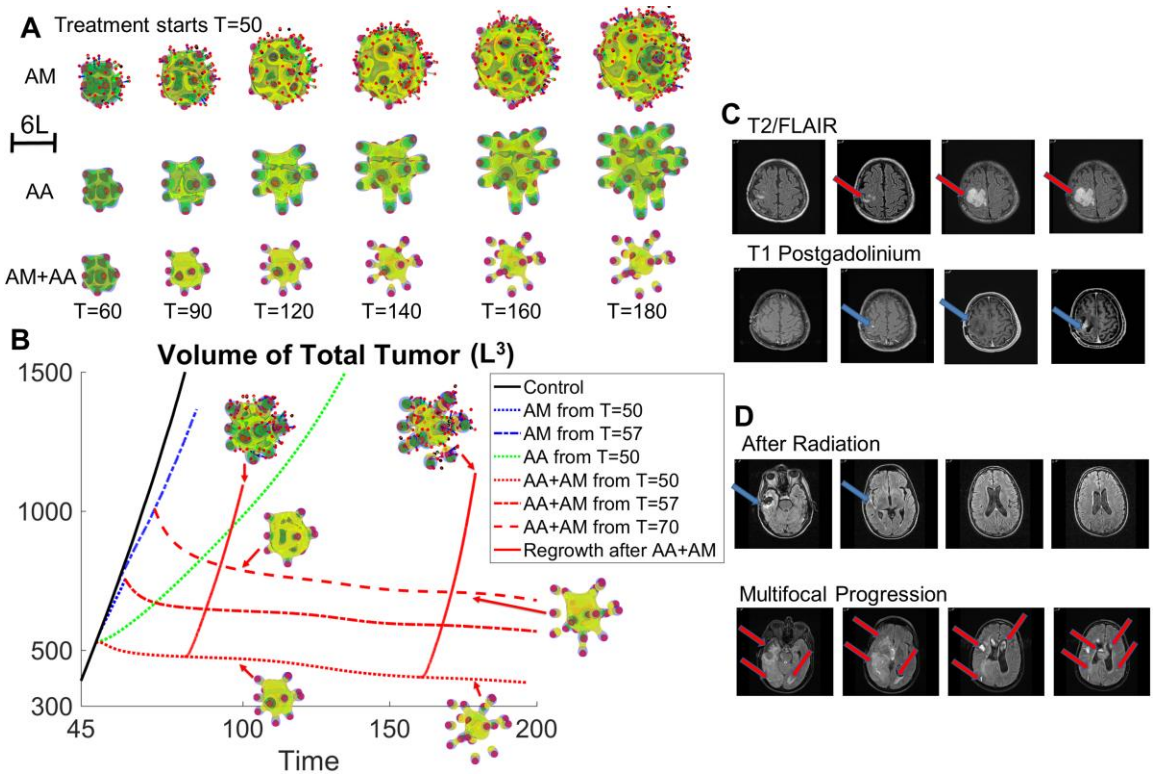

Fig. S5. Anti-angiogenic and anti-mitotic therapy reduce tumor size but increase invasiveness. **(A)** Evolution of a tumor treated with anti-mitotic therapy (AM) and/or anti-angiogenic therapy (AA). The tumor growth is identical to Fig. S2A until T=50. At T=50, the indicated therapy is applied. AM: the background vasculature releases an anti-mitotic agent that kills tumor cells proportionally to their mitosis rate. AA: the vasculature is completely removed and new vessels are not allowed to form. **(B)** Evolution of tumor volume in Fig. S2A (Control) and (A). Dotted line: AA (green), AM (blue) or AA+AM (red) is applied from T=50. Dot-dashed line: tumor growth is identical to Control until T=57 (tumor surface area has increased by 25% from T=50), then AM (blue) or AA+AM (red) is applied. Dashed red: tumor growth is identical to Control until T=57, then AM is applied until T=70 (tumor surface area increases 25% from T=57), then AA+AM is applied. Solid red: tumor regrowth after AA+AM is removed. Insets show tumor cells and vasculature after regrowth, compared to those treated with continued AA+AM. **(C)** Anti-angiogenic therapy increases invasion. Left column: minimal residual after surgery;

second column: progression after radiation and temozolomide. Third column: progression after bevacizumab. Right column: progression after bevacizumab. **(D)** Multifocal, dramatic progression in a patient who has received both bevacizumab and cytotoxic chemotherapy (irinotecan).

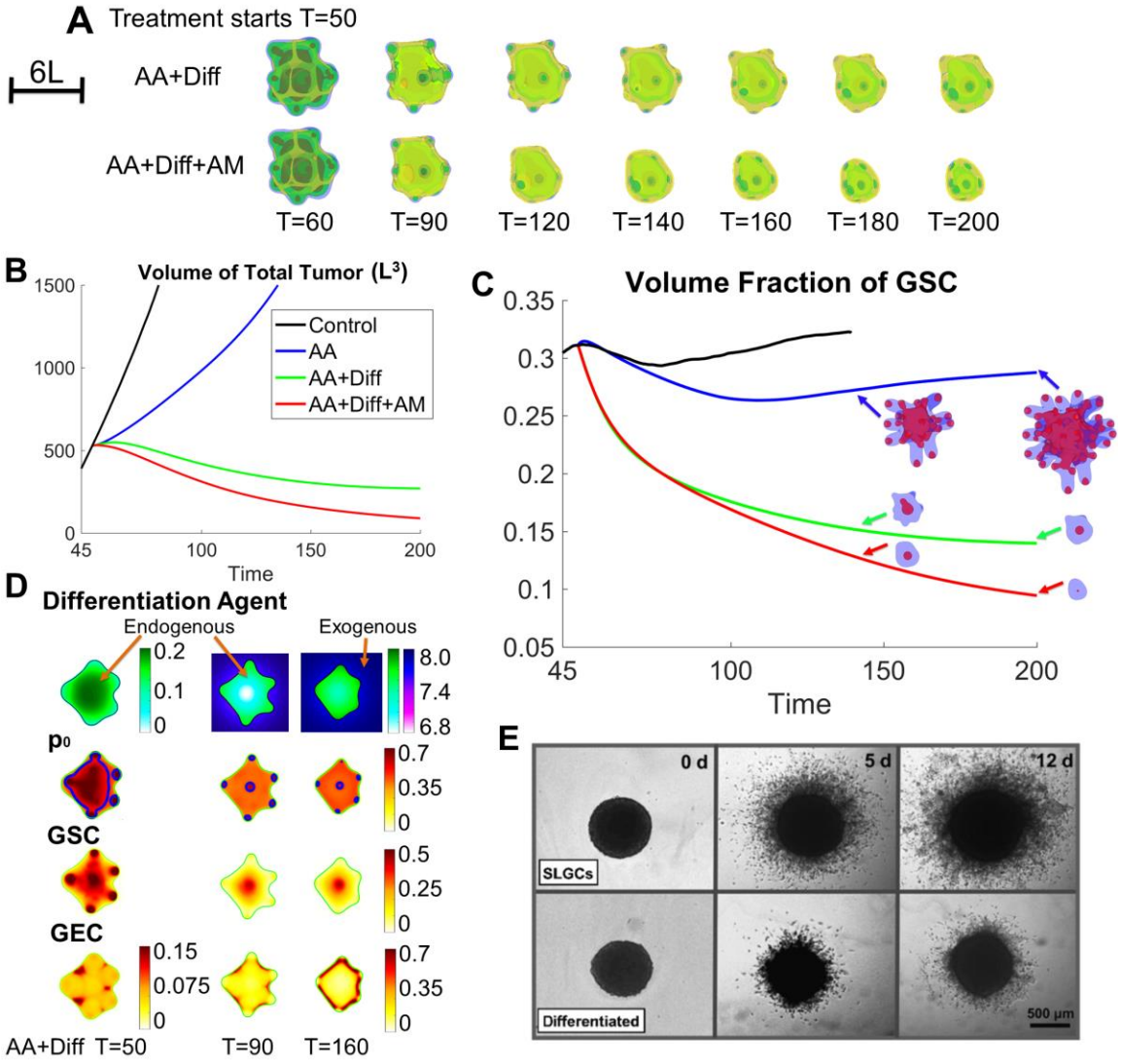

Fig. S6. Differentiation therapy reduces both tumor volume and invasion. **(A)** Evolution of tumors treated with anti-angiogenic (AA) and differentiation therapy (Diff), and/or anti-mitotic therapy (AM). The growth is identical to Fig. S2A until T=50. At T=50, the indicated therapy begins to apply. **(B-C)** Evolution of tumor volumes and GSC fractions

of tumors in Fig. S2A and (A). Insets in (C) show the distributions of GSC (red) in the tumor (blue). **(D)** 2D slices at the center of computational domain, of the differentiation agent, GSC self-renewal fraction (p_0), GSC and GEC in the tumor treated by AA+Diff. **(E)** Differentiation therapy reduces the invasiveness of stem-like glioma cells (SLSC), adapted from (2). Reprinted with permission.

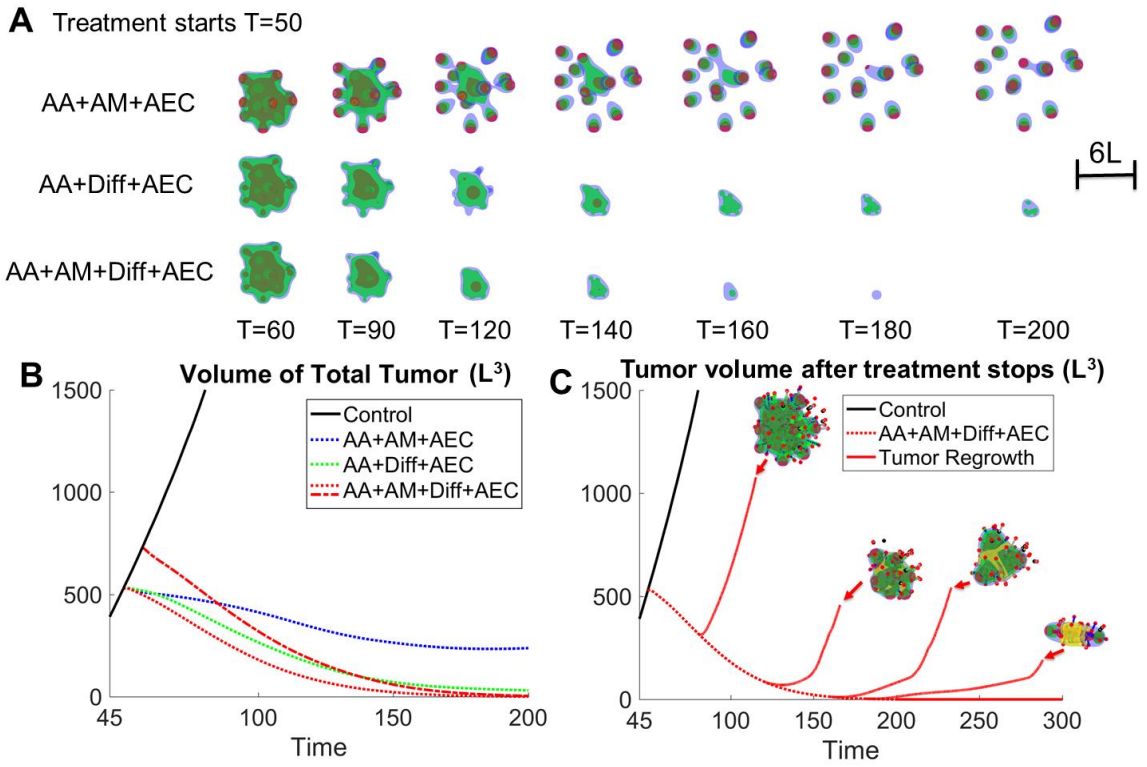

Fig. S7. Combinatorial therapies that can effectively reduce tumor size and invasiveness, and eventually kill the tumor. **(A)** Evolution of tumors treated by anti-angiogenic (AA) and anti-GEC therapy (AEC), combined with anti-mitotic therapy (AM) and/or differentiation (Diff) therapies. The growth is identical to Fig. S2A until T=50. At T=50, the indicated therapy is applied. AA+AM+AEC reduces growth but enhances invasiveness, while AA+Diff+AEC reduces both size and invasiveness. AA+AM+Diff+AEC for sufficient time (T=200) eventually eliminates the tumor. **(B)** Evolution of total volumes of tumors in Fig. S2A and (A). Dotted line: continuous treatment from T=50. Dot-dashed line: tumor

growth is identical to Control until T=57 followed by continuous treatment. **(C)** Evolution of tumor volume after the combined treatment (AA+AM+Diff+AEC) stops at T=80, 120, 160, 180 or 200, and the tumor vasculature is allowed to reform. Dotted red: continuous treatment from T=50; solid red: tumor regrowth after the treatment stops. Insets show the vasculature and tumor after regrowth. When AA+AM+Diff+AEC is applied through T=200, the tumor is removed and does not regrow even after the treatment stops.

Sec. S2. Model nondimensionalization and parameters.

We follow the nondimensionalization in (3). Let L and T be the length and time scale respectively. We follow (4) and choose L to be the nutrient diffusion length $L = \sqrt{D_n/u_n^{GSC}}$. Since the nutrient concentration is measured against that in the vasculature, we nondimensionalize n as $n' = n/\bar{n}$. Denoting $\nabla' = \nabla/L$ as the dimensionless gradient, we rewrite the equation for the dimensionless nutrient concentration n':

$$0 = \Delta' n' - (\varphi_{GSC} + u'^{GCP}_n \varphi_{GCP} + u'^{GTD}_n \varphi_{GTD} + d'_n)n + (p'^{H}_n Q(\varphi_T) + p'^{V}_n \rho_{FV})(1 - n'),$$

where $u'^{GCP}_n = u^{GCP}_n/u^{GSC}_n$, $u'^{GTD}_n = u^{GTD}_n/u^{GSC}_n$, $d'_n = d_n/u^{GSC}_n$, $p'^{H}_n = p^{H}_n/u^{GSC}_n$ and $p'^{V}_n = p^{V}_n/u^{GSC}_n$.

Next, we nondimensionalize the mass conservation equations Eq. (1). Let $t' = t/T$ be the dimensionless time, $\boldsymbol{u}' = \boldsymbol{u}/(L/T)$, $M' = M/\bar{M}$ and $\mu' = \mu/\bar{\mu}$ be the nondimensionalized cell velocity, mobility and chemical potential respectively. We rewrite the equation for φ_T as

$$\frac{1}{T\lambda^{GCP}_m \bar{n}}\left(\frac{\partial \varphi_T}{\partial t'} + \nabla' \cdot (\boldsymbol{u}'\varphi_T)\right) = \frac{\bar{M}\bar{\mu}}{L^2 \lambda^{GCP}_m \bar{n}} \nabla' \cdot (M'^{\varphi_T} \nabla' \mu') + \lambda'^{GSC}_m n' \varphi_{GSC} + n' \varphi_{GCP} - \lambda'_L \varphi_D.$$

We choose time scale $T = (\lambda^{GCP}_m \bar{n})^{-1}$ and $\frac{\bar{M}\bar{\mu}}{L^2 \lambda^{GCP}_m \bar{n}} = 1$. $\lambda'^{GSC}_m = \lambda^{GSC}_m/\lambda^{GCP}_m$, $\lambda'_L = \lambda_L/\lambda^{GCP}_m$.

Analogously, the dimensionless equations for other cell species are

$$\frac{\partial \varphi_{GSC}}{\partial t'} + \nabla' \cdot (\boldsymbol{u}'\varphi_{GSC}) = \nabla' \cdot (M'\varphi_{GSC} \nabla' \mu') + \lambda'^{GSC}_m n' \varphi_{GSC}(2p_0 - 1),$$

$$\frac{\partial \varphi_{GCP}}{\partial t'} + \nabla' \cdot (\boldsymbol{u}'\varphi_{GCP}) = \nabla' \cdot (M'\varphi_{GCP} \nabla' \mu') + \lambda'^{GSC}_m n' \varphi_{GSC} 2(1 - p_0 - r) + n' \varphi_{GCP}(2p_1 - 1),$$

$$\frac{\partial \varphi_{GEC}}{\partial t'} + \nabla' \cdot (\boldsymbol{u}'\varphi_{GEC}) = \nabla' \cdot (M'\varphi_{GEC} \nabla' \mu') + \lambda'^{GSC}_m n' \varphi_{GSC} 2r,$$

$$\frac{\partial \varphi_{GTD}}{\partial t'} + \nabla' \cdot (\boldsymbol{u}' \varphi_{GTD}) = \nabla' \cdot (M' \varphi_{GTD} \nabla' \mu') + n' \varphi_{GCP} 2(1 - p_1) - \lambda'^{GTD}_a \varphi_{GTD},$$

$$\frac{\partial \varphi_D}{\partial t'} + \nabla' \cdot (\boldsymbol{u}' \varphi_D) = \nabla' \cdot (M' \varphi_D \nabla' \mu') + \lambda'^{GTD}_a \varphi_{GTD} - \lambda'_L \varphi_D.$$

Here $\lambda'^{GTD}_a = \lambda'^{GTD}_a / \lambda^{GCP}_m$.

The dimensionless velocity $\boldsymbol{u}'$ satisfies $\frac{L}{T}\boldsymbol{u}' = -\frac{\bar{p}}{L}\nabla' p' + \frac{\bar{\mu}}{L}\mu' \nabla' \varphi_T$, where $p' = p/\bar{p}$ is the dimensionless pressure. We choose $\bar{p} = \bar{\mu} = \frac{L^2}{T}$, then

$$\boldsymbol{u}' = -(\nabla' \mathrm{p}' - \mu' \nabla' \varphi_T), \mu' = \frac{\gamma}{\varepsilon}(f'(\varphi_T) - \varepsilon^2 \nabla'^2 \varphi_T).$$

The dimensionless equation for C_V is

$$0 = \Delta' C_V - d'_V C_V + p'_V H(\tilde{n} - n)(\varphi_T - \varphi_D)$$

where $d'_V = L^2 d_V / D_V$ and $p'_V = L^2 p_V / D_V$. Analogously, we nondimensionalize the equations for C_{T1} and C_{T2}:

$$0 = \Delta' C_{T1} - \left(u'^{GSC}_{T1} \varphi_{GSC} + d'_{T1}\right) C_{T1} + p'_{T1} \varphi_{GTD}$$

$$0 = \Delta' C_{T2} - \left(u'^{GSC}_{T2} \varphi_{GCP} + d'_{T2}\right) C_{T2} + p'_{T2} \varphi_{GTD}$$

where $u'^{GSC}_{T1} = L^2 u^{GSC}_{T1} / D_{T1}$, $d'_{T1} = L^2 d_{T1} / D_{T1}$ and $p'_{T1} = L^2 p_{T1} / D_{T1}$. The parameters for C_{T2} are defined similarly.

The dimensionless equation for C_F is

$$\frac{\partial C'_F}{\partial t'} + \nabla' \cdot (\boldsymbol{u}'_w C'_F) = \Delta' C'_F + \left(p'^V_F \rho_V + p'^{GEC}_F \varphi_{GEC}\right) \cdot (1 - C'_F) - d'_F C'_F,$$

where $C'_F = C_F / \overline{C_F}$, $\boldsymbol{u}'_w = \boldsymbol{u}_w / (L/T)$, $d'_F = \frac{L^2}{T D_F} d_F$ and $p'_F = \frac{L^2}{T D_F} p_F$. Analogously, the dimensionless equation for C_W and C_{WI} are

$$\frac{\partial C_W}{\partial t'} + \nabla' \cdot (\boldsymbol{u'}_{\boldsymbol{w}} C_W) = D'_W \Delta' C_W + Src'_W,$$

$$\frac{\partial C_{WI}}{\partial t'} + \nabla' \cdot (\boldsymbol{u'}_{\boldsymbol{w}} C_{WI}) = D'_{WI} \Delta' C_{WI} + Src'_{WI},$$

where $D'_W = D_W T/L^2$ and $D'_{WI} = D_{WI} T/L^2$. We take source terms

$$Src'_W = k' \left(\frac{C_W^2}{C_{WI}} n' \varphi_{GSC} - d'_W C_W - u'_0 n' (\varphi_T - \varphi_D) \right)$$

$$Src'_{WI} = k' (p'_{WI} C_W^2 n' \varphi_{GSC} - d'_{WI} C_{WI})$$

where $\mathrm{k}' = \frac{T}{L^2 p_w \bar{n}} k$, $d'_W = \frac{d_W}{p_W \bar{n}}$, $u'_0 = \frac{u_0}{p_W \bar{n}}$, $p'_{WI} = \frac{p_{WI}}{p_W}$ and $d'_{WI} = \frac{d_{WI}}{p_W \bar{n}}$.

The parameters for the tumor in Fig. 2 in Main Text are listed below.

General Parameters		
Cell Mobility	$M = 10.0$	From (4).
Adhesion force	$\gamma = -0.1$	
Diffuse interface thickness	$\varepsilon = 0.05$	
Tumor Species		
GSC mitosis rate	$\overline{\lambda_m^{GSC}} = 0.7$	We follow (5) and assume that the GSC division rate is similar to that for dividing non-GSC cells (here, this is the GCP population). λ_m^{GCP}, Nondimensionalization parameter. Typically on the
GCP mitosis rate	$\lambda_m^{GCP} = 1.0$	
GTD death rate	$\lambda_a^{GTD} = 0.28$	
Dead cell lysis rate	$\lambda_L^D = 1.41$	

		order of 24 hours (5). λ_a^{GTD} and λ_L^D obtained by numerical experimentation. Results are qualitatively similar for a wide range of these parameter choices.
Feedback control		
Minimum GSC self-renewal probability	$p_0^{min} = 0.2$	See (4).
Maximum GSC self-renewal probability	$p_0^{max} = 1.0$	
Positive feedback gain on p_0 by C_W	$\chi_0^W = 1.0$	
Negative feedback gain on p_0 by C_{T_1}	$\psi_0 = 0.1$	
Maximum fold change of λ_m^{GSC}	$\Delta_m^F = 1.0$	From (6), which suggested that the crosstalk increases GSC proliferation by 50% to 100%. Magnitudes of feedback gains determined by numerical experiments. Results are qualitatively similar for a wide range of these parameter choices.
Positive feedback gain on λ_m^{GSC}	$\chi_m^F = 2.0$	
Positive feedback gain on p_0 by C_F	$\chi_0^F = 2.0$	
Minimum GCP self-renewal probability	$p_1^{min} = 0.2$	Parameters obtained by numerical experimentation. As long as $p_1^{max} < 0.5$, the
Maximum GCP self-renewal probability	$p_1^{max} = 0.45$	
Positive feedback gain on p_1 by C_W	$\chi_1^W = 1.0$	

Negative feedback gain on p_1 by C_{T2}	$\psi_1 = 0.1$	results are qualitatively similar for a wide range of these parameter choices.
Nutrient		
Diffusivity	$D_n = 0.5$	From (4).
Natural decay rate	$d_n = 1.0$	
Uptake rate by GSCs, GCPs and GTDs	$u_n = 1.0$	
Production rate by microenvironment	$p_n^H = 1.0$	
Production rate by functional vessels	$p_n^V = 1.0$	From (7).
VEGF		
Diffusivity	$D_V = 1.0$	From (7).
Natural decay rate	$d_V = 2.0$	
Production rate by all hypoxic cells	$p_V = 1.0$	
Hypoxic region threshold	$\tilde{n} = 0.5$	
Pattern formation		
Diffusivity of C_W	$D_W = 1.0$	From (4).
Production rate of C_W	$p_W = 1.0$	
Natural decay rate of C_W	$d_W = 1.0$	
Leak term of C_W	$u_0 = 0.2$	
Diffusivity of C_{WI}	$D_W = 25.0$	
Production rate of C_{WI}	$p_{WI} = 1.0$	
Natural decay rate of C_{WI}	$d_{WI} = 1.0$	
Reaction rate	$k = 25.0$	
Crosstalk factor C_{WF}		

Diffusivity	$D_F = 1.0$	Parameters obtained by numerical experimentation. Results are qualitatively similar for a wide range of these parameter choices.
Natural decay rate	$d_F = 1.0$	
Production rate by vasculature	$p_F = 0.2$	
Negative feedback factors		
Diffusivity	$D_{T1} = D_{T2} = 1.0$	From (4).
Production rate by GTDs	$p_{T1} = p_{T2} = 1.0$	
Uptake rate of C_{T1} by GSCs	$u_{T1}^{GSC} = 0.1$	
Uptake rate of C_{T2} by GCPs	$u_{T1}^{GCP} = 0.1$	

Sec. S3. Numerical methods.

We solved the mathematical model using an adaptive nonlinear multigrid method described in (8). We used an implicit second order Crank-Nicholson scheme for time discretization. Spatial derivatives were discretized using central difference approximations. Equations at the implicit time step were reformulated as a system of second order equations. Block structured Cartesian refinement was used to efficiently resolve the multiple spatial scales, especially in regions with large gradients (typically around tumor boundary). Tumor statistics, spatial distributions of cell species and vessel networks were generated by MATLAB.

Sec. S4. Detailed analysis of antiangiogenic and antimitotic therapies.

In this section, we first describe our implementation of antimitotic therapy (AM), and show the time evolution of tumors with antiangiogenic therapy (AA), AM and AA+AM in Figs. S8-S10. Then, we show the statistics of these tumors in Fig. S11, and the effects of AA on nutrient distribution and GSC in Fig. S12.

We assume that an antimitotic agent C_{CT} is produced by the background and tumor vasculature, and increases the death rates of all tumor cell species. We take

$$\frac{\partial C_{CT}}{\partial t} + \nabla \cdot (u_w C_{CT}) = \nabla(D_{CT} C_{CT}) + p_{CT}\varphi_H - d_{CT} C_{CT} - \left(u_{CT}^{GSC}\varphi_{GSC} + u_{CT}^{GCP}\varphi_{GCP} + u_{CT}^{GTD}\varphi_{GTD} + u_{CT}^{GEC}\varphi_{GEC}\right) C_{CT},$$

where D_{CT}, d_{CT} and p_{CT} are the diffusivity, natural decay and production rates by the host φ_H, respectively. u_{CT}^{i} is the update rate by cell type i, where $i = GSC, GCP, GTD$ or GEC. In addition, we assume that the death rates of GSC and GCP are proportional to their effective mitosis rate, $\lambda_m^{GSC} n$ and $\lambda_m^{GCP} n$ respectively. GEC die proportionally to the transdifferentiation rate *r*. The GTD death rate is positively regulated by C_{CT} from base rate $\widetilde{\lambda_a^{GTD}}$:

$$\lambda_a^{GSC} = \lambda_m^{GSC} n \cdot \frac{1}{2}\frac{C_{CT}}{1 + C_{CT}}$$

$$\lambda_a^{GCP} = \lambda_m^{GCP} n \cdot \frac{1}{2}\frac{C_{CT}}{1 + C_{CT}}$$

$$\lambda_a^{GTD} = \widetilde{\lambda_a^{GTD}}\left(1 + \frac{1}{2}\frac{C_{CT}}{1 + C_{CT}}\right)$$

$$\lambda_a^{GEC} = r \cdot \frac{1}{2}\frac{C_{CT}}{1 + C_{CT}}.$$

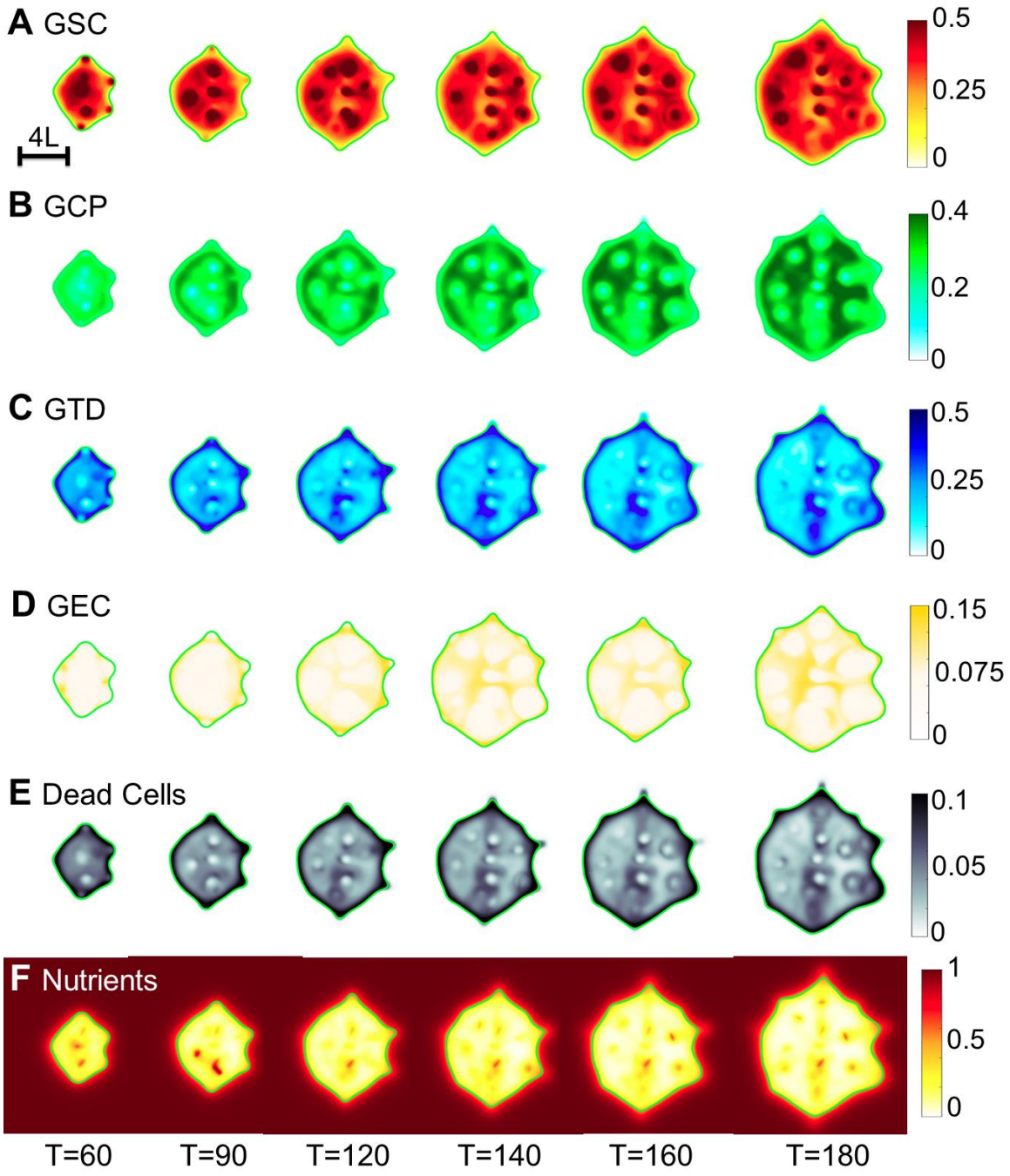

Fig. S8. Detailed analysis of tumor with antimitotic (AM) therapy. The 2D slices of GSC, GCP, GTD, GEC, DC and nutrients at *z=0* are shown at indicated times. Functional vessels produce nutrients in the tumor that enhance cell proliferation. In addition, tumor vasculature also produces the crosstalk factor that increases GSC self-renewal (see also Fig. S12), resulting in multiple GSC clusters at the tumor center.

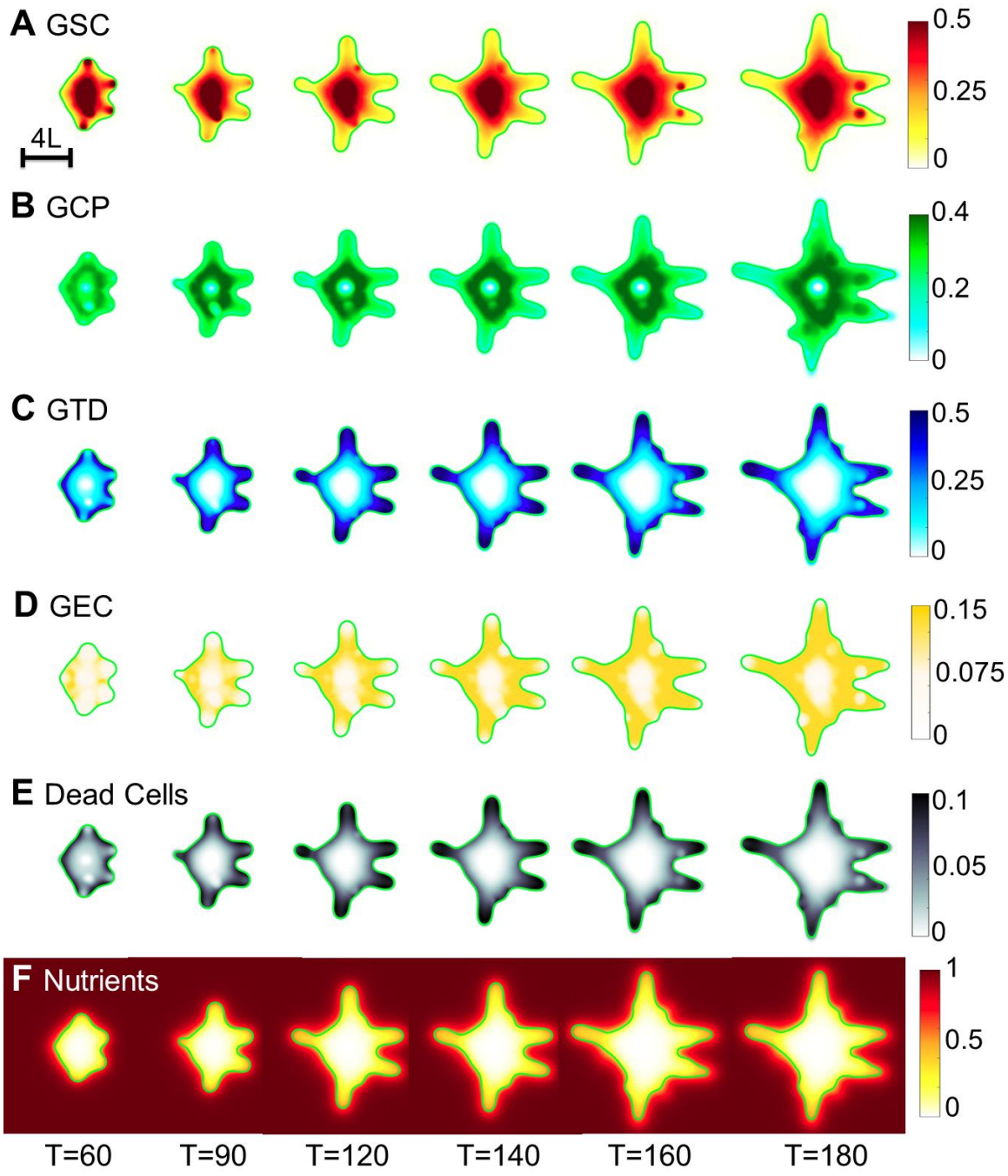

Fig. S9. Detailed analysis of tumor with antiangiogenic (AA) therapy. The 2D slices of GSC, GCP, GTD, GEC, DC and nutrients at *z=0* are shown at indicated times. AA removes all tumor vasculature, which reduces nutrient concentrations in the tumor. The fingers grow considerably, increasing tumor surface area and the access to nutrients.

The GSC cluster at tumor center persists, because GSC mitosis is inhibited by reduced nutrient concentration, and GSC are self-sustained, see Fig. S12.

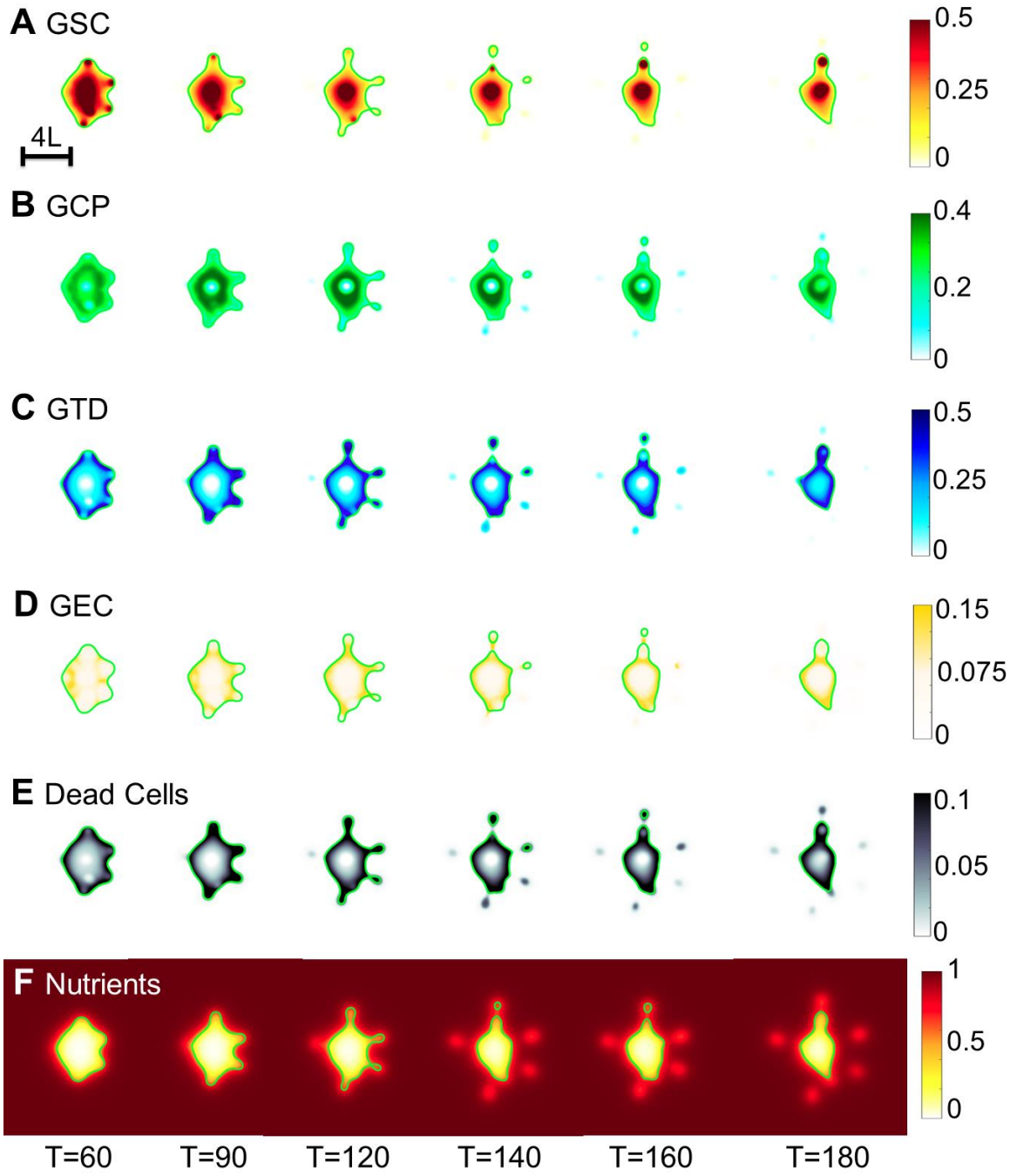

Fig. S10. Detailed analysis of tumor treated by both AM and AA. The 2D slices of GSC, GCP, GTD, GEC, DC and nutrients at *z=0* are shown at indicated times. While AA prompts the fingers to grow, AM kills cells at finger necks, resulting in multifocal tumors.

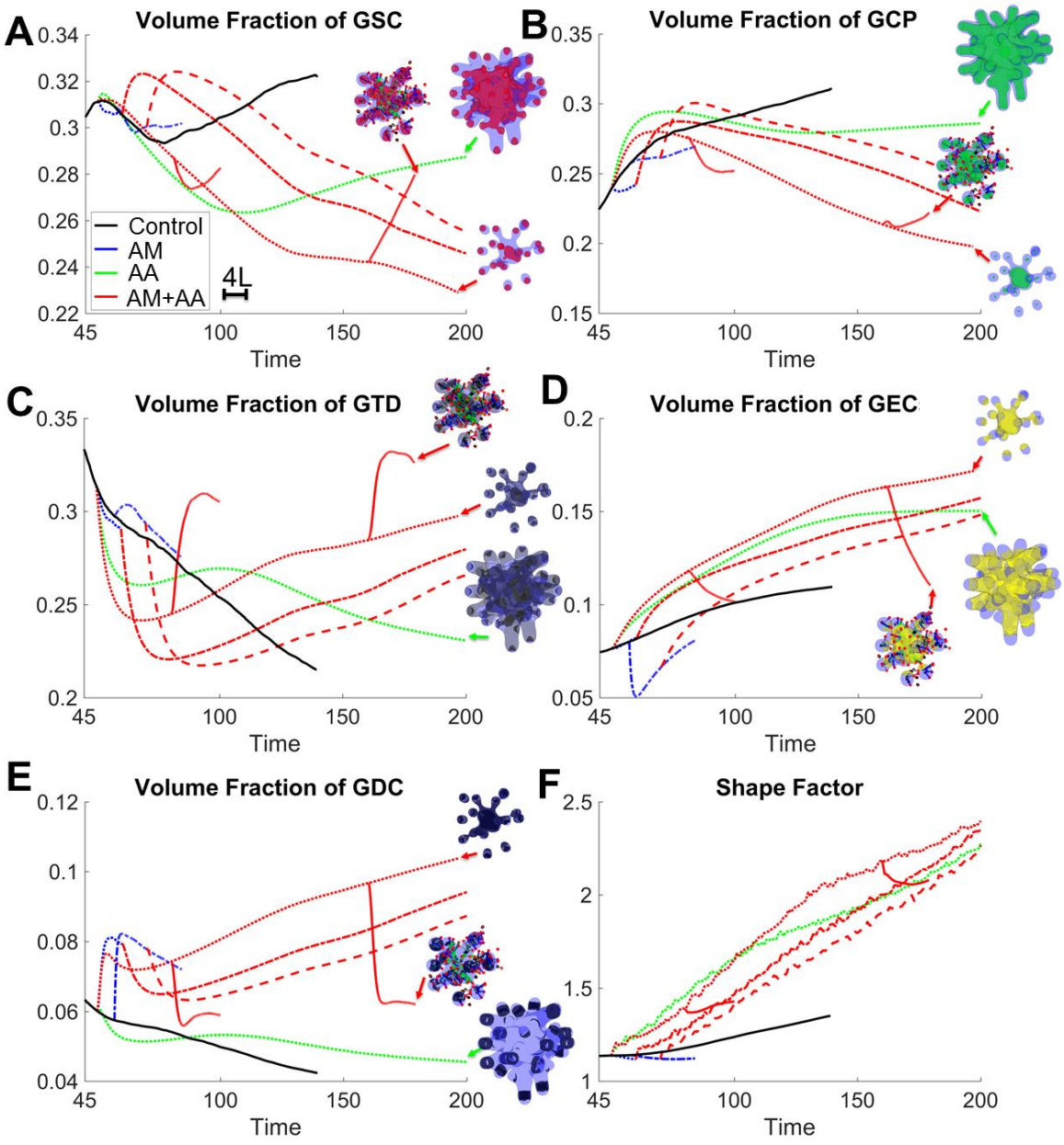

Fig. S11. Detailed analysis of antiangiogenic (AA) and antimitotic (AM) therapies. **(A-E)** Volume fraction of GSC, GCP, GTD, DC and GEC. Insets show the corresponding cell

type in the tumor. AA decreases the GSC fraction by removing the vasculature-GSC crosstalk. Applying AM further decreases the fraction, which recovers when the treatment is removed. **(F)** Tumor shape factor calculated by $\sqrt[3]{36\pi}\frac{S}{V^{2/3}}$ where V is the tumor volume and S is the surface area. Larger shape factor indicates more irregular tumor shape and greater invasiveness. The shape factor of a sphere is one. Applying AM alone decreases the shape factor, whereas AA results in prolonging fingers and significantly increases the shape factor. Applying both AM and AA results in multifocal tumors and further increases the shape factor.

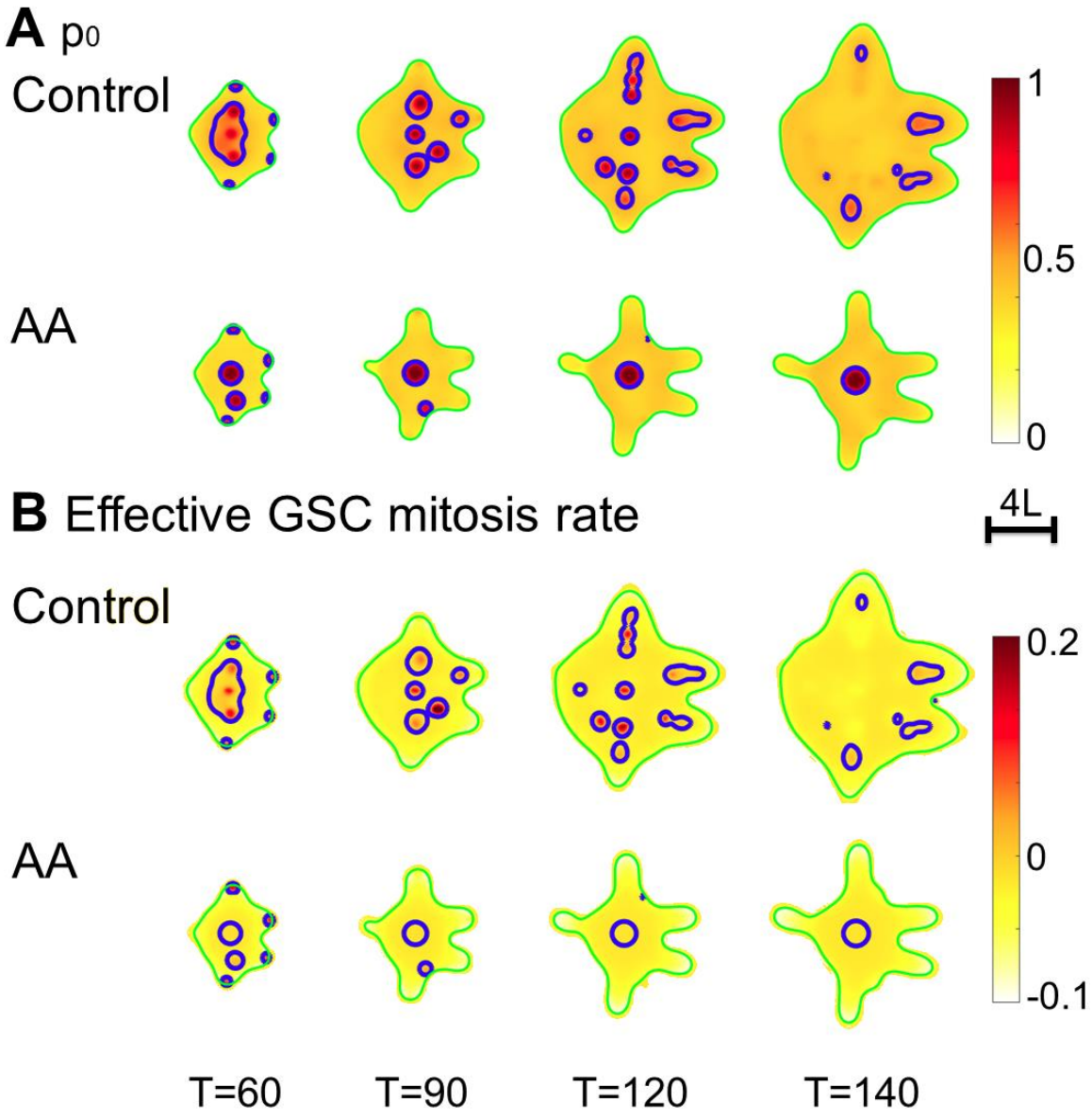

Fig. S12. 2D slices of p_0 and effective GSC mitosis rate $\lambda_m n(2p_0-1)$ of Control and the tumor treated by AA, at *z=0* and indicated times. Green: tumor boundary; blue: $p_0=0.5$ or $\lambda_m n(2p_0-1)=0$ contour. In Control, the vasculature releases nutrients and the crosstalk factor that enhance GSC mitosis. In AA, after the vasculature is removed at T=50, the GSC cluster at the center is self-sustained ($p_0>0.5$).

Sec. S5. Detailed analysis of anti-GSC therapies.

In this section, we first describe our implementation of differentiation therapy (Diff), then show the time evolution of tumors with AA+Diff or AA+Diff+AM in Figs. S13-S14. Next, we analyze the statistics of these tumors in Fig. S15. We then investigate different levels of Diff in Fig. S16. In Fig. S17, we show that similar effects can be achieved by inhibiting GSC self-renewal promotor Wnt.

Implementation of differentiation therapy

We assume that the background vasculature releases the GSC differentiation promotor in addition to its endogenous production. In particular, we take

$$0 = \nabla^2 C_{T1} - \left(d_{T1} + u_{T1}\varphi_{GSC}\right)C_{T1} + p_{T1}^{GTD}\varphi_{GTD} + p_{T1}^{H}\varphi_{H},$$

where p_{T1}^{H} is the production rate of C_{T1} by the background vasculature. Analogously, we implement the Wnt-Inhibitor treatments as follows:

$$\frac{\partial C_{WI}}{\partial t} + \nabla \cdot (u_w C_{WI}) = \nabla(D_{WI} C_{WI}) + \bar{\gamma}(p_{WI} C_W^2 n \varphi_{SC} - d_{WI} C_{WI} + p_{WI}^{H}\varphi_H),$$

where p_{WI}^{H} is the production rate of C_{WI} by the background vasculature.

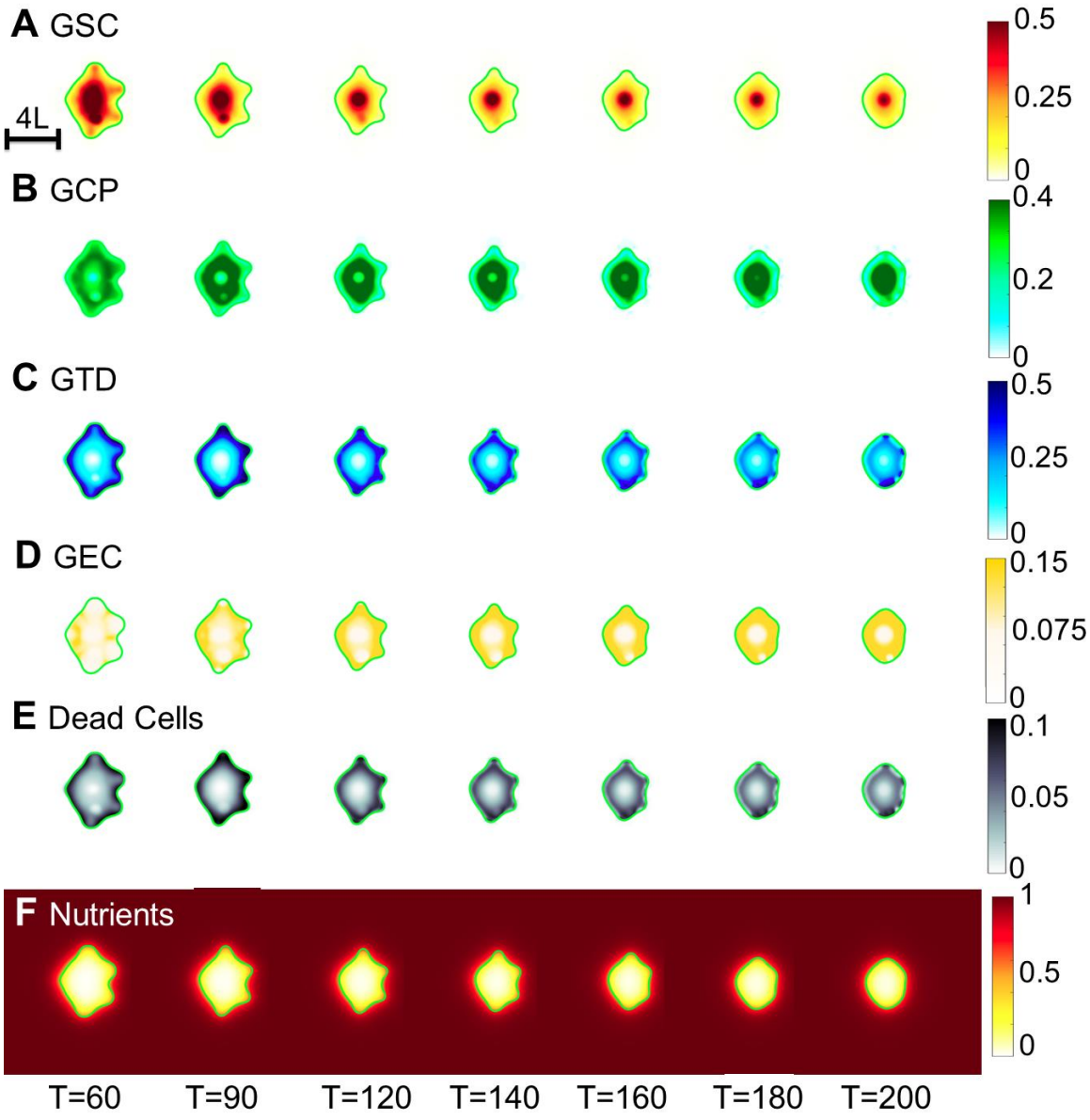

Fig. S13. Detailed analysis of tumor treated by both AA and Diff. The 2D slices of GSC, GCP, GTD, GEC, DC and nutrients at *z=0* are shown at indicated times. Diff forces all GSC clusters near tumor boundary to differentiate, resulting in compact tumor shapes. However, GSC at tumor center are protected by GEC surrounding tumor boundary (see Fig. 6 (D) in the main text). The tumor volume is reduced initially, but stabilizes at late times.

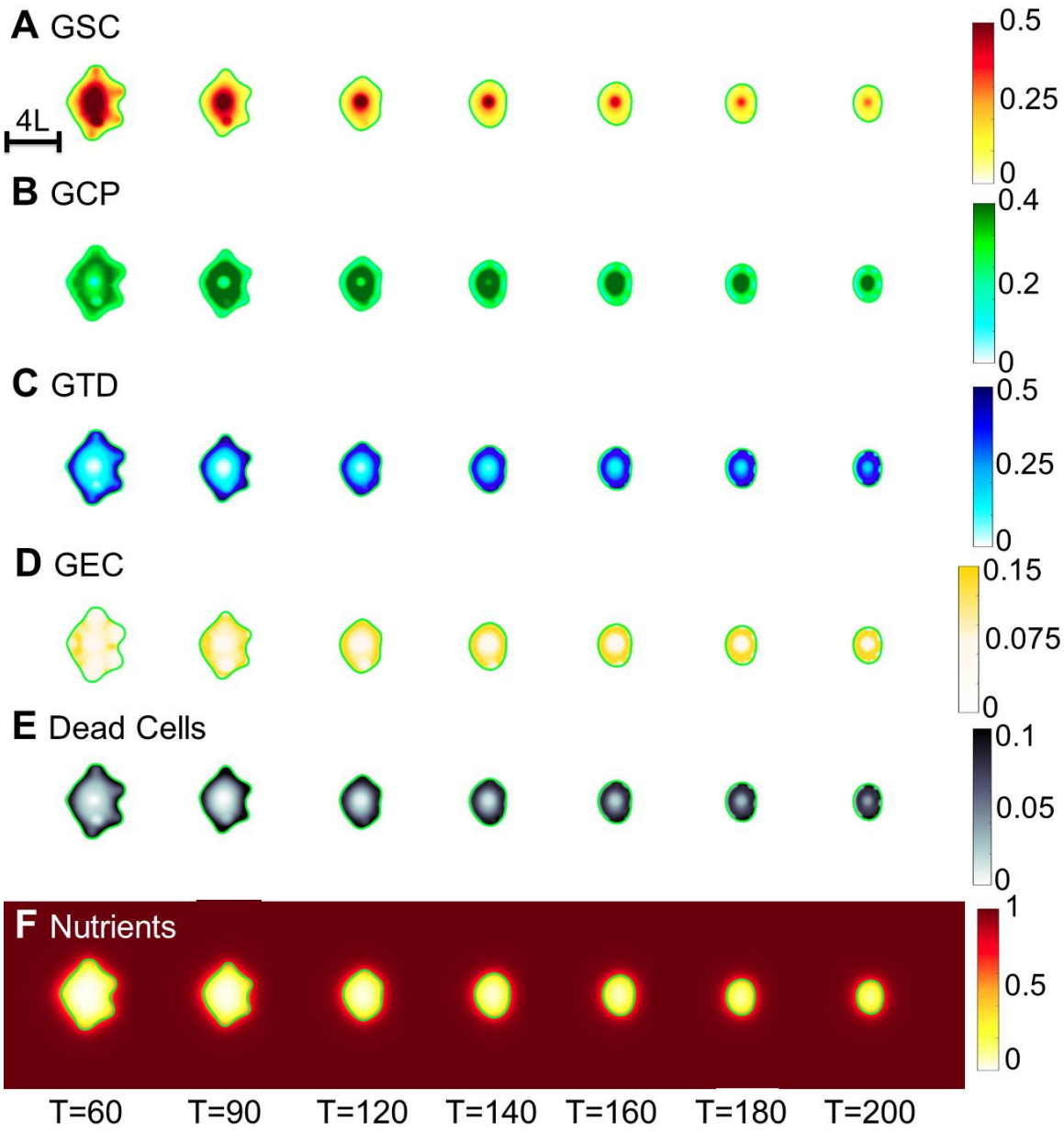

Fig. S14. Detailed analysis of tumor treated by AA, AM and Diff. The 2D slices of GSC, GCP, GTD, GEC, DC and nutrients at *z=0* are shown at indicated times. The cell distributions are analogous to those in Fig. S13. AM kills all tumor cells and further reduces tumor size.

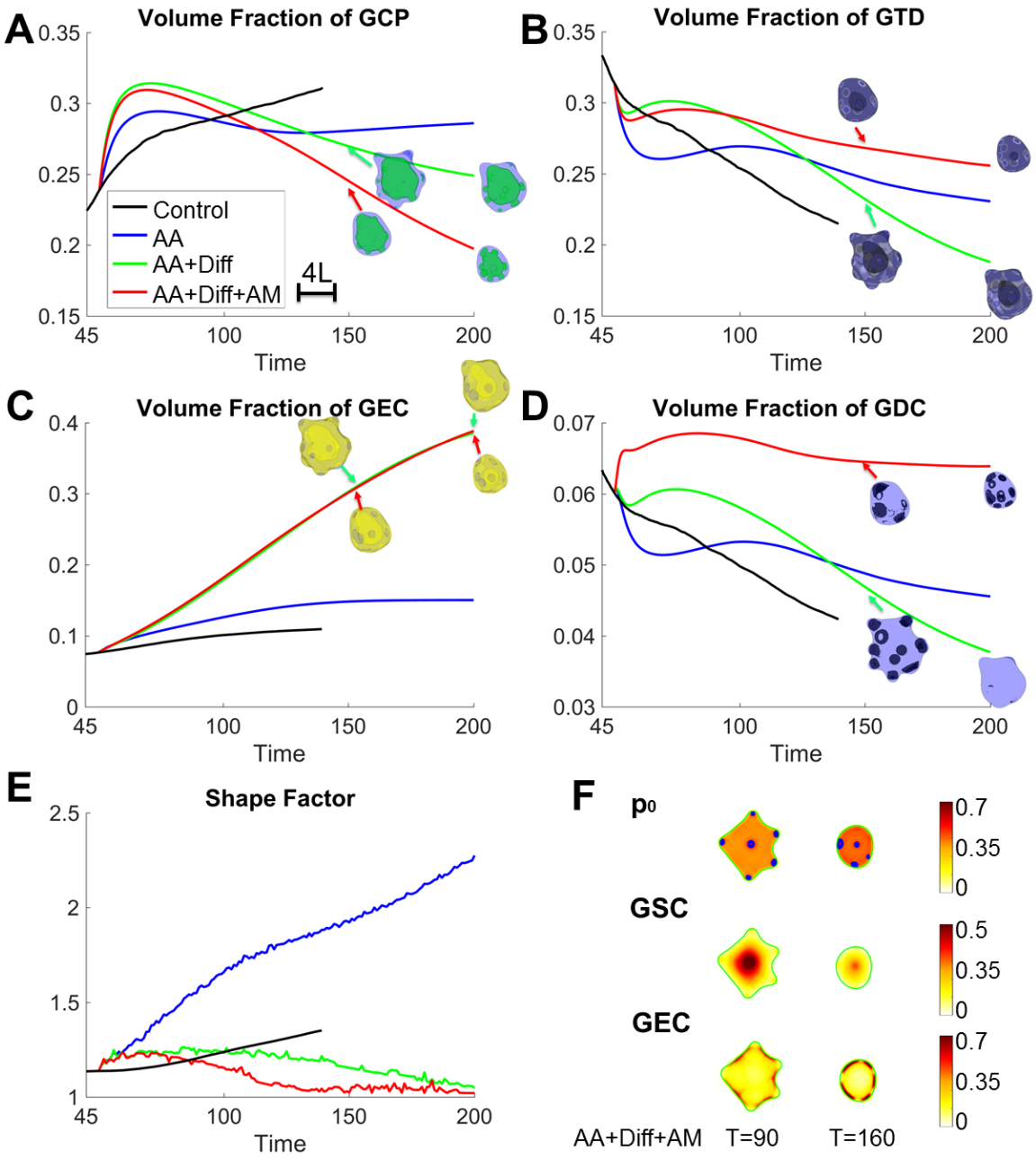

Fig. S15. Detailed analysis of differentiation therapy (Diff) and/or chemotherapy (AM). **(A-D)** Volume fraction of GCP, GTD, DC and GEC. Insets show the corresponding cell type in the tumor. In Fig. 6, GEC begin to cover the tumor boundary when Diff is applied. The GEC fraction increases accordingly. **(E)** Evolution of tumor shape factor. In contrast to AA that increases tumor invasion, Diff reduces the shape factor by inhibiting finger

development, since Diff forces GSC at finger tips to differentiate. **(F)** 2D slices at *z=0*, of GSC self-renewal fraction p0, GSC and GEC in the tumor treated by AA+Diff+AM.

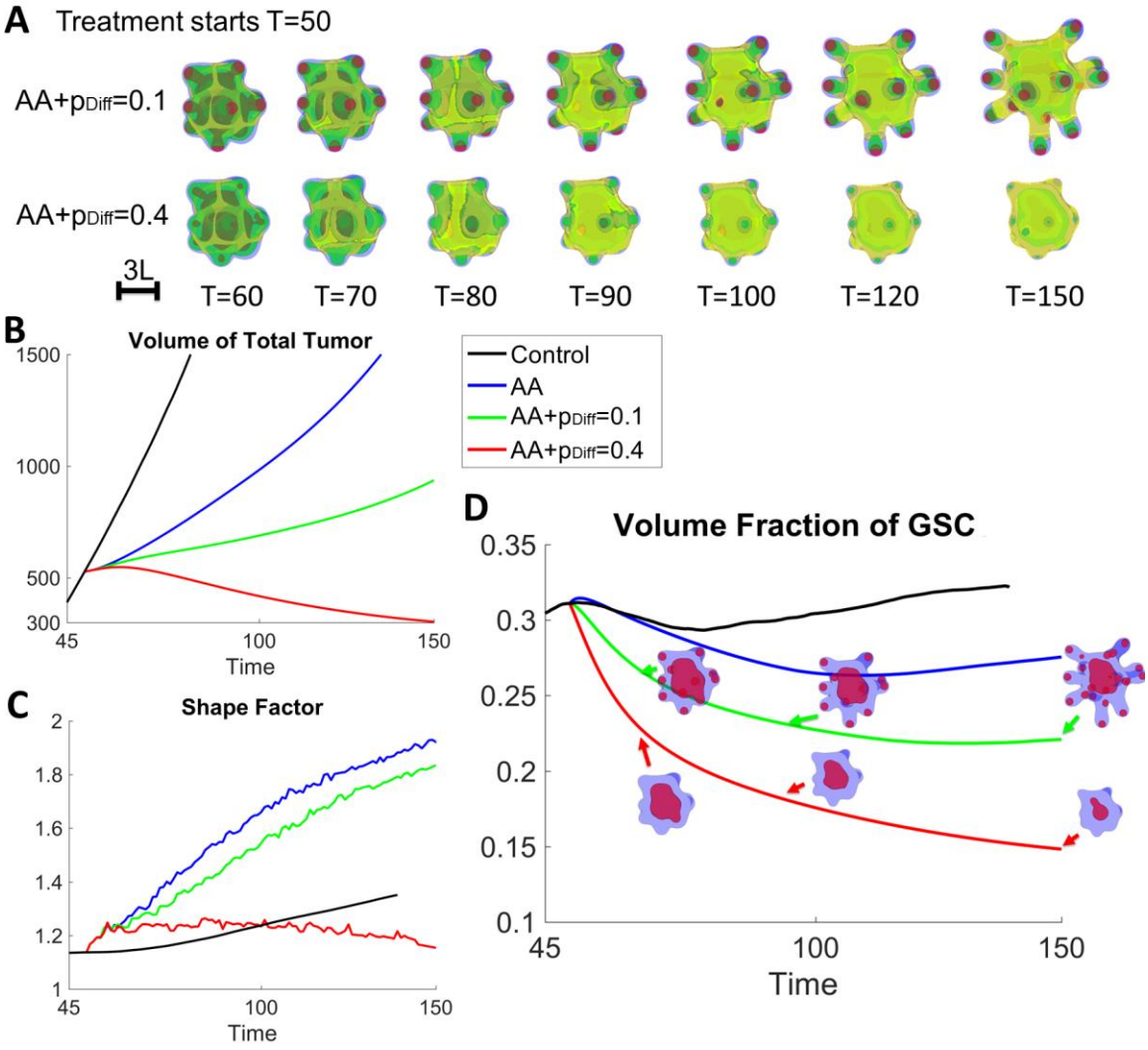

Fig. S16. Differentiation therapy (Diff) needs to be sufficiently large to control tumor invasion. **(A)** Evolution of tumors treated with anti-angiogenic (AA) and low to high levels of Diff (blue: tumor boundary; red: φ_{GSC}=0.3; green: φ_{GCP}=0.25; yellow: φ_{GEC}=0.1). The growth is identical to Fig. 2A until T=50. At T=50, the indicated therapy begins to apply. **(B-D)** Evolution of tumor volumes, shape factor and GSC fractions. Insets in (D) show the distribution of GSC (red) in the tumor (blue). Low levels (p_{Diff}=0.1) of Diff reduces the

shape factor but cannot prevent fingers from growing. Higher level (p_{Diff}=0.4, the value used in the main text) removes GSC clusters from finger tips and inhibits finger development. The GSC fraction is further decreased.

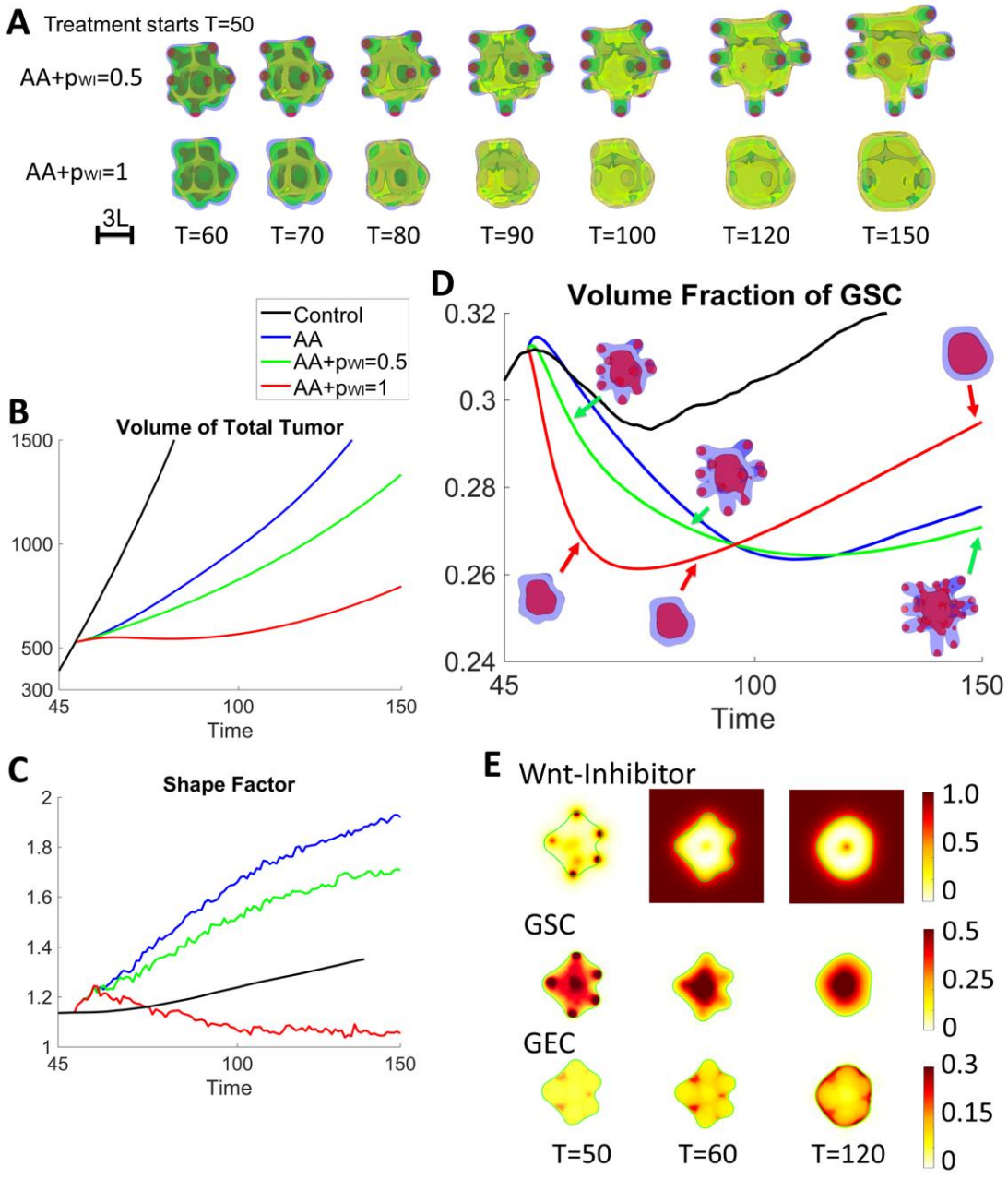

Fig. S17. Inhibiting Wnt has similar effects with differentiation therapy. **(A)** Evolution of tumors treated with anti-angiogenic (AA) and low to high levels of Wnt-Inhibitor (WI) produced by the background vasculature. The growth is identical to Fig. 2A until T=50.

At T=50, the indicated therapy begins to apply. **(B-D)** Evolution of tumor volumes, shape factor and GSC fractions. Similar to low levels of differentiation therapy, a small amount of WI (p_{WI}=0.5) reduces the shape factor but fingers continue to develop. Larger amount of WI (p_{WI}=1) removes GSC clusters from tumor surface and stops finger development. The tumor grows in a compact shape. **(E)** 2D slices of WI, GSC and GEC in the tumor with p_{WI}=1 are shown at indicated times. Similar to the differentiation therapy, GEC cover the tumor boundary. Consequently, the WI treatment cannot remove the GSC cluster at the tumor center.

Sec. S6. Detailed analysis of anti-GEC and combinatorial therapies.

In this section, we first describe our implementation of anti-GEC therapy (AEC), then show the time evolution of tumors with AA+AM+AEC, AA+Diff+AEC or AA+AM+Diff+AEC in Figs. S18-S20. Next, we analyze the statistics of these tumors in Fig. S21.

Similar to chemotherapy, we assume that the background vasculature releases an agent C_L that increases the death rate of GEC. We take

$$\frac{\partial C_L}{\partial t} + \nabla \cdot (u_w C_L) = \nabla(D_L C_L) + p_L \varphi_H - d_L C_L + u_L \varphi_{GEC} C_L,$$

where D_L, d_L, p_L and u_L are the diffusivity, natural decay, production rates by the host and uptake rate by GEC respectively. The death rate of GEC is positively regulated by C_L from a base rate $\widetilde{\lambda_a^{GEC}}$:

$$\lambda_a^{GEC} = \widetilde{\lambda_a^{GEC}} \cdot \frac{C_L}{1 + C_L}.$$

When the antimitotic therapy is also applied, we take

$$\lambda_a^{GEC} = \widetilde{\lambda_a^{GEC}} \cdot \frac{C_L}{1 + C_L} + r \cdot \frac{1}{2} \frac{C_{CT}}{1 + C_{CT}}.$$

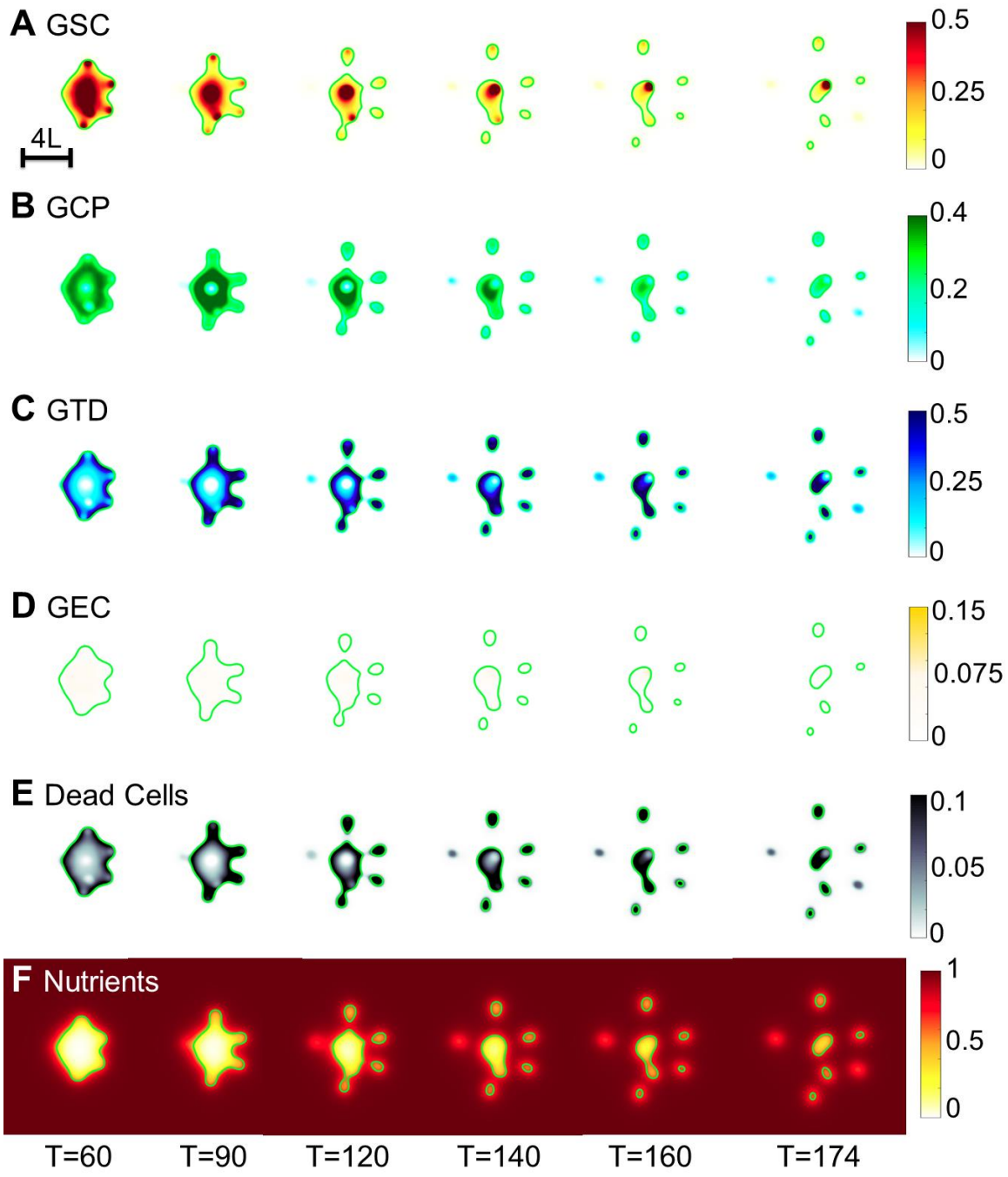

Fig. S18. Detailed analysis of tumor treated by AA, AM and AEC. The 2D slices of GSC, GCP, GTD, GEC, DC and nutrients at *z=0* are shown at indicated times. When AA and AM are applied together, the tumor become multifocal (see Fig. S10) and invasive. Here, AEC kills GEC at finger necks (compare (D) to Fig. S3 (D)) and further increase tumor invasiveness.

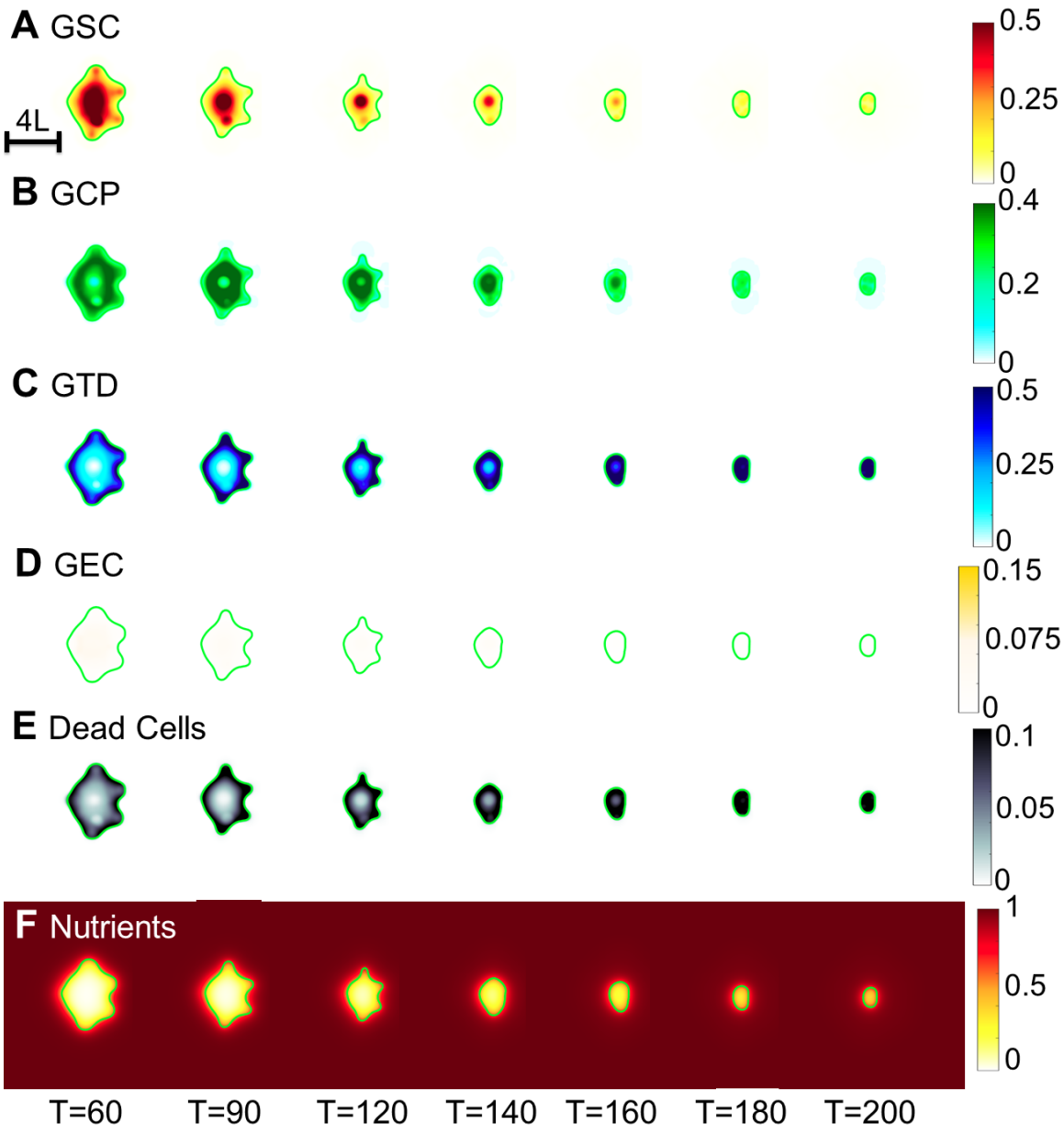

Fig. S19. Detailed analysis of tumor treated by AA, Diff and AEC. The 2D slices of GSC, GCP, GTD, GEC, DC and nutrients at *z=0* are shown at indicated times. When AA and Diff are applied together, the tumor grows in a compact shape and the volume is reduced. However, the GSC cluster at tumor center persists. Here, AEC removes GEC surrounding the tumor boundary (compare (D) and Fig. S13(D)), and Diff effectively forces GSC at tumor center to differentiate. Consequently, the tumor volume is reduced.

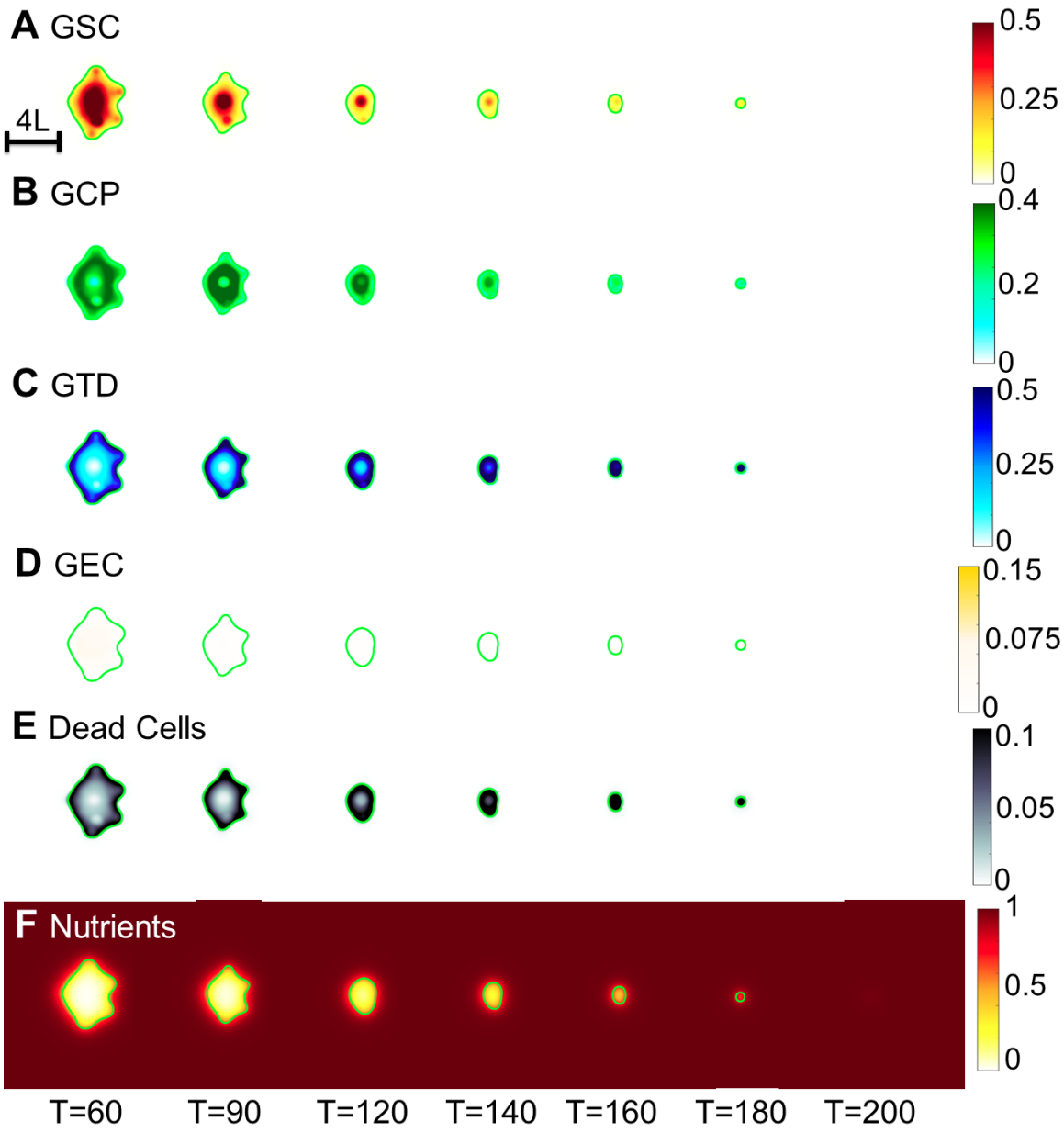

Fig. S20. Detailed analysis of tumor treated by AA, AM, Diff and AEC. The 2D slices of GSC, GCP, GTD, GEC, DC and nutrients at *z=0* are shown at indicated times. The cell distributions are analogous to those in Fig. S19. AM kills viable tumor cells and further reduces tumor volume. At T=200, the tumor has been killed.

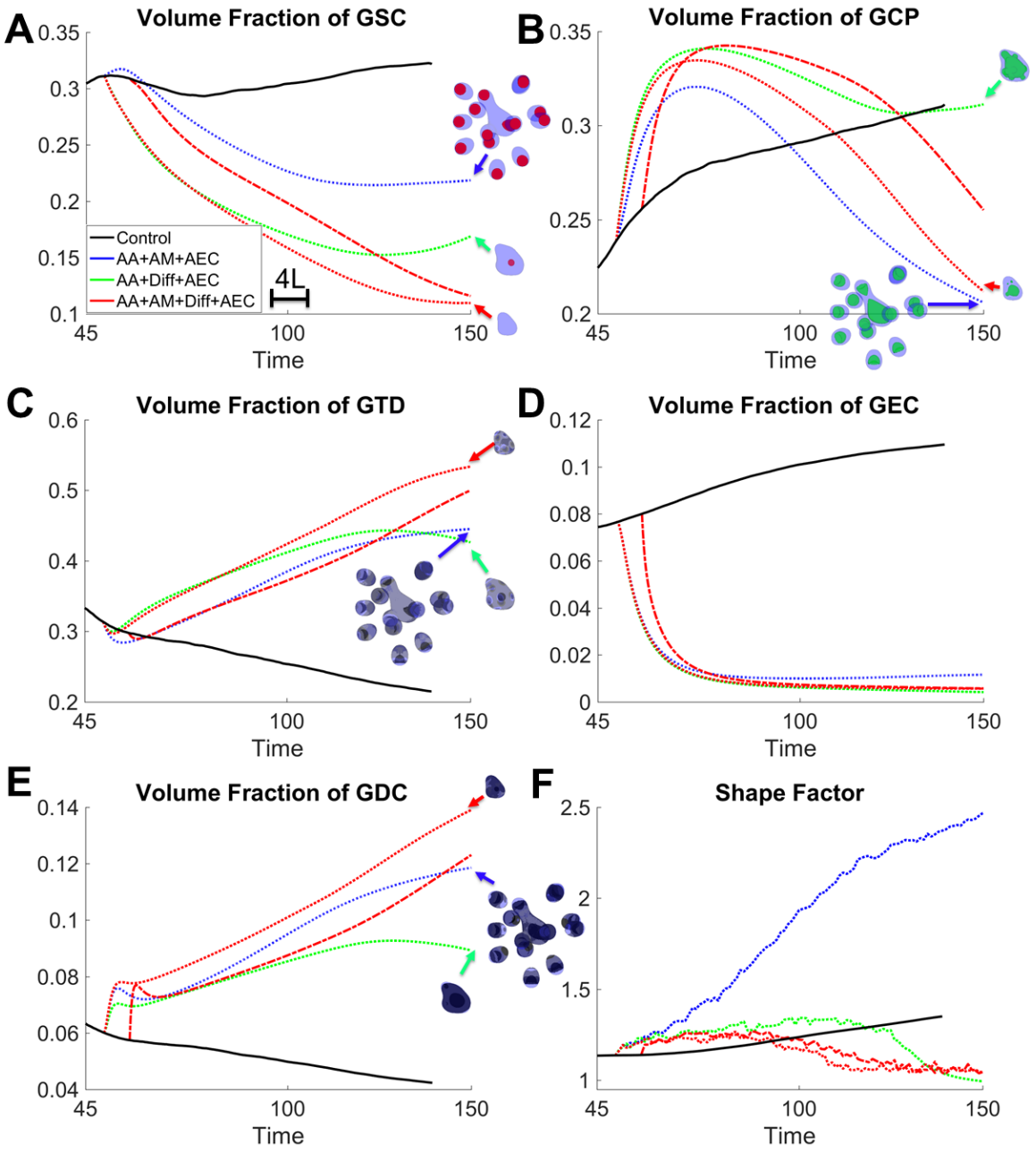

Fig. S21. Detailed analysis of combinatorial therapies targeting transdifferentiated GEC. **(A-E)** Volume fraction of GSC, GCP, GTD, DC and GEC. Insets show the corresponding cell type in the tumor. **(F)** Evolution of tumor shape factor. AEC kills almost all GEC, removing the positive feedback on GSC self-renewal via the crosstalk factor. Consequently, the GSC fractions are decreased. When treated by AA, AM and AEC, the

tumor is multifocal and much more invasive. Applying Diff effectively reduces tumor size and the tumor grows in a compact shape.

References

1. Kaijun Di MEL, Daniela A. Bota. TRIM11 is over-expressed in high-grade gliomas and promotes proliferation, invasion, migration and glial tumor growth. Oncogene **2013**;32:5038-47
2. Campos B, Wan F, Farhadi M, Ernst A, Zeppernick F, Tagscherer KE*, et al.* Differentiation therapy exerts antitumor effects on stem-like glioma cells. Clin Cancer Res **2010**;16:2715-28
3. Yan HR-L, M.; Frieboes, H. B.; Hughes, C. C. W.; Lowengrub, J. S. Multiscale Modeling of Glioblastoma Suggests that the Partial Disruption of Vessel/Cancer Stem Cell Crosstalk Can Promote Tumor Regression Without Increasing Invasiveness. IEEE Transactions on Biomedical Engineering **2017**;64:538-48
4. Youssefpour H, Li X, Lander AD, Lowengrub JS. Multispecies model of cell lineages and feedback control in solid tumors. Journal of theoretical biology **2012**;304:39-59
5. Gao X, McDonald JT, Hlatky L, Enderling H. Acute and fractionated irradiation differentially modulate glioma stem cell division kinetics. Cancer Res **2013**;73:1481-90
6. Borovski T VJ, ten Cate R, Cameron K, de Vries NA, van Tellingen O, Richel DJ, van Furth WR, Medema JP, Sprick MR. Tumor microvasculature supports proliferation and expansion of glioma-propagating cells. Int J Cancer **2009**;125:1222-30

7. Frieboes HB, Jin F, Chuang YL, Wise SM, Lowengrub JS, Cristini V. Three-dimensional multispecies nonlinear tumor growth-II: Tumor invasion and angiogenesis. J Theor Biol **2010**;264:1254-78

8. Wise SM, Lowengrub JS, Cristini V. An Adaptive Multigrid Algorithm for Simulating Solid Tumor Growth Using Mixture Models. Math Comput Model **2011**;53:1-20